Deep Learning Based Antenna Design and Beam-Steering Capabilities for Millimeter-Wave Applications

AHMED M. MONTASER[1] **AND KORANY R. MAHMOUD**[2,3], **(Senior Member, IEEE)**

[1]Electrical Engineering Department, Faculty of Technology and Education, Sohag University, Sohag 82524, Egypt
[2]Department of Electronics and Communications, Faculty of Engineering, Helwan University, Cairo 11795, Egypt
[3]National Telecommunications Regulatory Authority, Ministry of Communication and Information Technology, Giza 71515, Egypt

Corresponding author: Korany R. Mahmoud (kurany_hameda@h-eng.helwan.edu.eg)

ABSTRACT In this study, a deep neural network (DNN) is implemented to soft computation of the dual-band circularly polarized bone-shaped patch antenna (BSPA) at 28 GHz and 38 GHz for 5G applications. Via a simulated database of 150 BSPAs, a DNN model is constructed on a 5-layer system using an adaptive learning rate algorithm. The framework and hyper-parameters of the DNN model are optimized in the training phase of a hybrid algorithm combining strengths of both particle swarm optimization (PSO) and a modified version of the gravitational search algorithm (MGSA-PSO). To generate the database for training and testing the model, 150 BSPAs with different geometrical are simulated in terms of the resonant frequency using a precise electromagnetic analysis platform. A fabricated BSPA operating at 28 GHz and 38 GHz is used to test and verify the DNN model. Then, the application of DNN with back-propagation algorithm and weighted MGSA-PSO algorithm is used for beam-steering the main beam pattern of the designed uniform circular antenna array with side-lobe level $<= -30$ dB by estimating the appropriate feeding phases of the 16 elements. Several illustrative examples are placed to beam-steer the pattern in the desired direction to check the validity of the technique.

INDEX TERMS Deep learning, artificial neural network, optimization algorithm, mm-wave antennas, circular polarization, beamforming technique.

I. INTRODUCTION

Recently, the demand for increased capacity in mobile and personal communications systems in addition to other modern applications such as satellite and, multi-input multi-output (MIMO) networks, biomedical imaging, remote sensing, radio astronomy, and radar, have motivated researchers towards the development of algorithms and standards that exploit space selectivity [1]. In this regard, one pertinent problem is finding antenna rotation for desired beam direction. Many techniques have been used to steer an antenna's radiation pattern over the years [2]. The mechanical phased arrays rotated with motors started in military applications several decades ago. But nowadays it became undesirable, especially when factors such as weight, antenna size, and weather conditions have been considered. In addition to its limited use in static or very slow-changing environments due to the limitation in steering speed [3]. Rotating mechanisms

The associate editor coordinating the review of this manuscript and approving it for publication was Oğuzhan Urhan.

are also prone to mechanical failure due to fatigue and the wearing of moving parts. The solutions for these problems led to electronic ways of steering beams. As a result, there are many efforts on the design of phased antenna array systems that play an important role in shaping and scanning the radiation pattern and constraining the adaptive algorithm used by the digital signal processor. These methods of beam steering based on controlling the phase values, the excitation amplitudes only, and both amplitudes and phases have been extensively considered in the literature [4]–[8]. The most important method is based on controlling the complex weights since the technique utilizes fully the degrees of freedom for the solution space. On the other hand, it is also considered the most expensive approach taking into consideration the cost of both phase shifters and variable attenuators for all elements. Therefore, beam pattern scanning based on controlling phase values was the only valid method in this work.

In literature, many papers studied the synthesis of antenna array using different optimization techniques, such as genetic algorithm [9], particle swarm optimization algorithm [10],

central force optimization [11], gravitational search algorithm [12], in addition to hybrid techniques those have been successfully used [5]–[8], [13]. However, the computational time to find the optimum weights will increase by considering more antenna array elements. Therefore, the deep neural network (DNN) is an essential computational tool with an unprecedented computational efficiency for these time-critical applications.

Recently there is a great effort by researchers to find easier and faster analysis techniques such as developed neural networks and optimization algorithms inspired by nature. Therefore, any computational system can find a relationship between inputs and outputs of an engineering system through the association of multiple layers of nodes and each node has its connection weight. This system is called the neural network [14]. The neural network has a high performance in accuracy and rapid if designed correctly. Even though in cases with large and computationally complex problems, their network structure may not be interconnected and deep enough to duly train the model. Hence, an urgent need for the emergence of DNNs, or as they are called deep learning, as a deep analytical method for difficult and complex simulated problems.

In the beginning, DNN was used in the field of image and speech recognition, as a modern tool for NN [15]. Recently, DNN has been used in many applications and its effectiveness has been proven with great success, for example, in antennas designs and beamforming capabilities. As for traditional neural networks, which can be described as shoal networks compared to the features provided by DNN, the DNN is more in-deep, complexity, number of layers, and neurons. In addition to an essential feature that distinguishes DNN from traditional NN, which is its ability to discover useful and new features of the input data. This, in turn, makes DNN have great computational depth and is more compatible with major, large-scale, and complex systems. Therefore, when DNN deals with difficult and complex problems that have a large amount of data, they need further computing engines to accelerate the process, such as a graphics processing unit. Moreover, a smart network such as DNN can perform many features such as simultaneous multi-layer processing, feature selection, and monitoring of certain excessive parameters. In the past few years, machine-learning scientists turned their attention to the astonishing results of DNN that they have achieved on the ground, particularly in audiovisual media research and prediction [16], so they decided to apply it to various engineering problems [17]–[19]. Recently, DNN is provided to different electromagnetic applications included antenna design, direction-of-arrival estimation, beamforming, multi-input multi-output systems, forward/inverse scattering, radar, and remote sensing due to its superior capabilities [20]–[24].

DNN can supply a hurried beamforming synthesis process while preserving high accuracy levels, minimizing error and time saving, and a possible prediction of the antenna behavior, a better computational efficiency, and a reduced

number of necessary simulations. Therefore, the proposed DNN model is an accurate and robust computing approach as an alternative to expensive measurement and simulation. [23] provides a detailed review of various research papers that address the design and optimization of antennas using machine learning, including the various techniques and algorithms used to produce antenna parameters based on desired radiation characteristics and other antenna specifications. Also, [24] presents a novel modified efficient K-Nearest Neighbors (KNN) method, the advantage of this method, which is considered a type of neural network, is the reduction in the number of training and testing data samples. When applying this method to a model (the parameters of this model are less than ten parameters), this model requires only a small number of samples (only from the 10 to 100 samples), for the dataset and some prior information at the beginning to constrain the target domain. Then comes the self-learn stage, and by using some types of rapid simulation, the optimum value can be predicted quickly and accurately. One of the important advantages of this method is its ability to generate more valuable data samples during the training process, so the efficiency of this method is very high.

The Multilayer Perceptron (MLP) with a single hidden layer is a big implication that has been emerged in recent years as interest in NNs has grown. Whenever a large number of hidden layer neurons are used, this network can predict any smooth nonlinear input-output mapping to an arbitrary degree of accuracy [25]. Radial basis function (RBF) neural networks are used in [26] to refine the radiation pattern of non-uniform linear arrays of high superconducting rectangular microstrip antennas. In [27], a phased array in a coordinated scheme based on Taguchi-neural networks is presented. The authors of [28] presented a typical use of back-propagation neural networks for antenna array synthesis and optimization.

In [29], the authors used an array 4×1 of the patch antenna with an inter-element space of 0.28λ for synthesizing the radiation patterns. A DNN was constructed with the input being the radiation pattern and the output being the amplitude and phase of the antenna elements. The proposed DNN has been trained with a large number of samples of radiation models that show reasonable performance in synthesizing the radiation patterns. The radiation pattern produced by DNN was quite similar to that of the input radiation. This proved that deep learning can be used surely for radiation pattern synthesis. In general, antennas are found to be ideal candidates for DNNs because of the intrinsic nonlinearities involved with their radiation patterns.

In this paper, a DNN-based model is optimized in the training phase of a hybrid MGSA-PSO algorithm for the dual resonant frequency computation of the bone-shaped patch antenna (BSPA) with an axial ratio (AR) < 3 dB. The accuracy of the model is further validated on a measured BSPA resonating at 28 GHz and 38 GHz simultaneously. Also, the DNNs are used to simplify the antenna array modeling by assessing phases. The key challenge is to find optimal antenna array element weights that result in
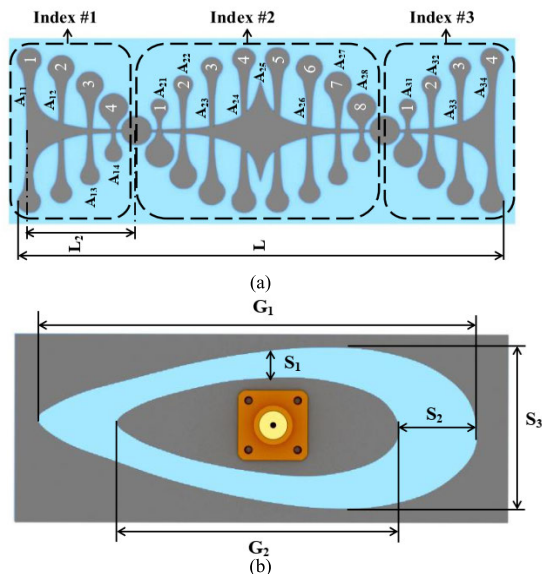
(a)

(b)

FIGURE 1. Proposed antenna structure (a) Top view, (b) Back view.
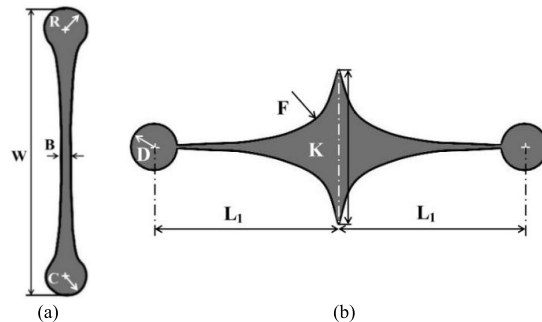

FIGURE 2. (a) Shape of bone structure, (b) Rhombus shape with a concave rib and a solid circle connects the groups to each other.

TABLE 1. The value of Initial and optimized dimensions (in millimeter).

Variable	W_{11}	W_{12}	W_{13}	W_{14}	W_{21}	W_{22}	W_{23}	W_{24}	W_{25}	W_{26}
Initial value	3.5	3.1	2.35	1.4	1.4	2.35	3.1	3.5	3.5	3.1
Optimum value	3.5	2.94	2.2	1.25	1.15	1.9	2.38	2.5	2.38	1.95
Variable	W_{27}	W_{28}	W_{31}	W_{32}	W_{33}	W_{34}	L	D	K	F
Initial value	2.35	1.4	1.4	2.35	3.1	3.5	10	0.4	2.1	7
Optimum value	2	0.8	0.7	1.1	1.4	1.59	9.9	0.38	1.9	6.57
Variable	L_1	B_{11}	C_{11}	S_2	G_2	L_2	R_{11}	S_1	G_1	S_3
Initial value	2.55	0.13	2.1	1.7	6.1	2.25	2.5	0.6	9.3	3.5
Optimum value	2.5	0.12	2	1.68	5.9	2.3	2.3	0.58	9.21	3.39

a beam-steering radiation pattern with a minimum side-lobe level (SLL) of less than −30 dB, thereby improving antenna array efficiency. To verify the validity of the technique, several illustrative examples are placed to beam-steering the pattern toward the desired direction. The paper is organized as follows. The antenna design and array configuration are presented in Section II. Deep neural networks are described in Section III. Section IV presents the results and discussions. Finally, Section VI makes conclusions.

II. DESIGNS AND CONFIGURATIONS
This section presents firstly the designed structure of the proposed dual-band and circularly polarized antenna element. Then, the geometrical arrangement of the uniform circular array consists of 16 antenna elements is introduced.

A. CONFIGURATION OF ANTENNA ELEMENT DESIGN
Fig. 1 shows the proposed antenna structure which consists of a bone-shaped linear array with sinusoidal length distribution and connected through periodic rhombus structures as shown in Fig. 1(a). The antenna ground plane consists of a perfect electric conductor (PEC) layer etched with an elliptical shape as illustrated in Fig. 1(b). Fig. 2(a) illustrates the shape of bone structure with thickness and overall length B and W, respectively. The radii of bone ends are R and C. The Rhombus shape with a concave rib and the solid circle which connects the groups is illustrated in Fig. 2(b) with the corresponding dimensions.

As depicted in Fig. 1(a), the antenna mainly consists of four bone shapes, which are A_{11}, A_{12}, A_{13}, A_{14}. They are arranged from largest to smallest, as shown in group index 1, and this group of bones is repeated twice in group index 2. The first time the lengths were repeated inversely, i.e. from the small to the large bone, and also the position was reversed, meaning that the left side replaces its right side and vice versa the right side replaces its left side A_{21}, A_{22}, A_{23}, A_{24}. Then

the group was repeated in the same order and placed group index 1, which are the bones A_{25}, A_{26}, A_{27}, A_{28}. Finally, we come to the last group, which is group index 3, which is reversed in lengths and position as the first iteration in-group index 2, which are A_{31}, A_{32}, A_{33}, A_{34}. A solid circle connects the groups, which greatly affects the current distribution and prevents eddy currents from occurring in the entire radiation patch. There is also a rhombus shape with a concave rib that starts from the beginning of the group index 2 to the end of this group. Half of this state-inverse rhombus are found in group index 1, and group index 2. So that the rhombus head faces the other in the solid circle that connects the groups. The purpose of having this rhombus is to increase the metallic area to the radiated patch, leading to a direct improvement in the antenna radiation efficiency. The antenna is fed by a coaxial cable 50 ohm at a point in the antenna structure's middle.

The antenna is designed then fabricated on the Rogers® Duroid™ RT5880 with a 0.508 mm substrate thickness, relative permittivity $\varepsilon_r = 2.2$, and loss tangent $tan\delta = 0.0009$ substrate. The antenna initial dimensions were illustrated in Table 1.

B. ANTENNA ARRAY DESIGN
In this work, a uniform circular array (UCA) antenna geometry is introduced as shown in Fig. 3. A strong justification for this selection is the symmetry possessed which provides UCAs with a major advantage: the ability to scan a beam azimuthally through 360° with little change in either the beam width or the SLL. The array consists of 16 CP elements of the optimized BSPA antenna operating at 28 and 38 GHz simultaneously. The elements are uniformly distributed in a circle configuration with inner ring radius $R_1 = 1.273\lambda$, with equal spacing of $r = 0.5\lambda$ between any two consecutive elements has been considered, where λ is the wavelength of 28 GHz.
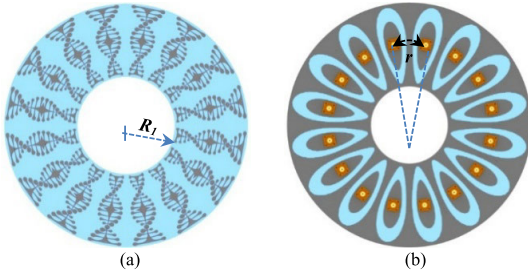
FIGURE 3. 2D view of UCA antenna structure, (a) front view, (b) back view.

The proposed 5G mm-wave antenna array is designed to synthesize the beam patterns in different directions. The radiation pattern can be steered in the desired direction with a high gain and a side-lobe level less than -30 dB by adjusting the phase of the input signal allocated to each antenna element. Therefore, the MGSA-PSO algorithm is considered to optimize the feeding phases for DNN learning.

III. DEEP NEURAL NETWORK (DNN)

Deep learning distinguishes itself from machine learning by combining feature collection and regression/classification, having a larger number of neurons, processing simultaneously on several layers, inherently extracting features, and evaluating optimum network hyperparameters. The data in the DNN system is evaluated by moving it through the neurons in the multi-layered hierarchy, and the evaluated information is then passed on to the next layers, allowing a more convenient learning model to be constructed.

In the beginning, we briefly introduce the DNN description that was applied to the BSPA design. Multilayer perceptions (MLPs) [31]–[33], which were successfully and frequently employed in many engineering applications, are favored in this investigation. Many algorithms, such as Levenberg-Marquardt (LM), backpropagation, and delta-bar-delta, can be used to train the MLP. MLPs are trained in this study using the GSA-PSO algorithm [6], [7], which has quick learning and high convergence capabilities. As shown in Fig. 4, the MLP has five layers: an input layer, an output layer, and three hidden layers. The neurons of the layer merely act as buffers for distributing the input signals x_i to the neurons of the hidden layer. Each hidden layer neuron j sums its input signals x_i after weighting them with the strengths of the respective input layer connections w_{ji}, and computes its output y_j as a function f of the sum, namely

$$y_j = f\left(\sum \omega_{ji} x_i\right) \quad (1)$$

where $f(\cdot)$ can be a simple threshold function, a sigmoid, hyperbolic tangent, a radial basis function, a purelin function, etc. [32], [33]. Similarly, the output of neurons in the output layer is computed. When training a network, one of the available learning algorithms is used to adjust the network's weights. At time t, the learning algorithm returns the change $\Delta\omega_{ji}(t)$ in the weight of a connection between neurons i and j. The weights for the LM learning algorithm are updated using
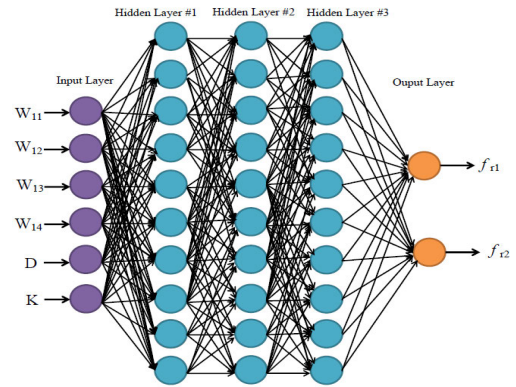

FIGURE 4. The proposed 5–layer DNN framework.

the formula below.

$$\omega_{ji}(t+1) = \omega_{ji}(t) - \Delta\omega_{ji}(t) \quad (2)$$

$$\Delta\omega_{ji} = [J^T(\omega)J(\omega) + \mu I]^{-1} J^T(\omega) E(\omega) \quad (3)$$

where, μ, I, and $E(\omega)$ are the Jacobian matrix, a constant, identity matrix, and error function, respectively. The Jacobian matrix contains the first derivatives of the errors with respect to the weights and biases. After each successful step, the value of μ is dropped, and it is only increased when a step would increase the sum of squares of errors. A DNN model with five layers was applied in this work, including the input layer, three hidden layers, and the output layer. The number of epochs in the training procedure is 150. In addition, the input layer, hidden layer, and output layer all used the tangent sigmoid, tangent sigmoid, and purlin functions, respectively.

Secondly, we applied DNN on a circular disk antenna array for beam-steering. As shown in Fig. 5, multi-layer networks have an input layer whose neurons code the information supplied to the network, a configurable number of "hidden" internal layers, and an output layer. In the same layer, neurons do not communicate with one another. These networks' learning process is supervised. The input nodes make up the first layer. A feed-forward neural network with one hidden layer and a Multilayer Perceptron MLP node function at each hidden node is known as an MLP network. The dimension of the input vector is equal to the number of nodes, L [34]–[36]. Where j is the input layer's index ($j = 1, 2, \ldots, L$) and i is the hidden layer's index ($I = 1, 2, \ldots, N$). With $k = 1, 2, \ldots, M$, k is the index of the output layer.

The interconnection weights are calculated using the minimal error between the neural model output y_k and the training data d_k. The goal of the training procedure is to fine-tune the network interconnection weights ω_{ij} and ω_{ki} in order to reduce the error function $E(p)$, which is defined as:

$$E(p) = \frac{1}{2}\sum_{k=1}^{M}\sum_{i=1}^{N}\sum_{j=1}^{L}[y_k(x_j, \omega_{ij}, \omega_{ki}) - d_k]^2 \quad (4)$$

where $p = 1, 2, \ldots, P$ denotes the training set's index. The back-propagation technique described in [27] is used in this iterative procedure. The weights ω_{ij} and ω_{ki} are updated for
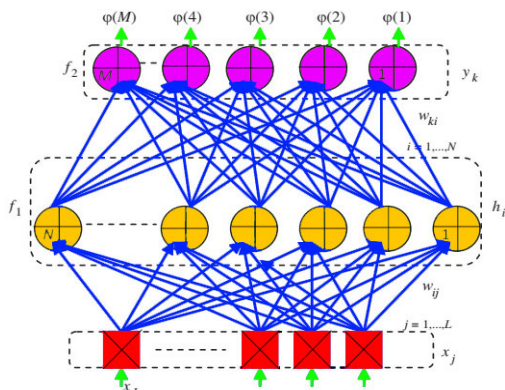
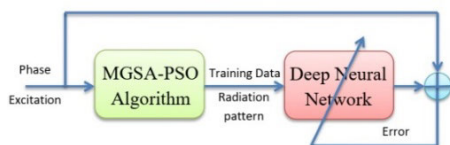**FIGURE 5.** The neural beam-former architecture.

FIGURE 6. Neural network training procedure.

each iteration by:

$$\Delta \omega_m = -\eta \frac{\partial E}{\partial \omega_m} \qquad (5)$$

Sector-width intervals of 15° and SLL intervals of − 30 dB were used in the training set. Fig. 6 depicts the mean square error performance of the MLP Network. The ability of neural networks to generalize is one of their main advantages. This means that even if a trained network has never seen data from the same class as the learning data, it will classify it. Developers of real-world applications typically only have access to a small portion of all possible patterns of neural network generation. The dataset should be divided into three sections to achieve the best generalization: The training set is used to train a neural network; during training, the dataset's error is minimized, the validation set is used to assess a neural network's success on patterns that have not been trained during the learning process and a test set for determining a neural network's overall efficiency.

In such a case, we have two main steps called network designing and network testing (generalization). In network designing, the input vectors $\{x_p, p = 1, 2, \ldots, 16\}$ is firstly formed, then generating input/output pairs $\{x_p, \varphi_q\}$, where $q = 1, 2, \ldots, 18$, then design the neural networks. In the network testing, we form the vectors $x'p$ for the testing input samples. Then present input vectors $x'p$ to the neural networks. Finally, we get the output of the network.

The number of hidden neurons chosen is heavily influenced by the essence of the nonlinearity to be modeled. In our situation, 30 hidden neurons ensured that the algorithm converged quickly and that the neural model we created was accurate as depicted in Table 2. The continuous nonlinear neuron, whose activation function is a tan sigmoid function, is the neuron employed in this network. To study the concepts described in the preceding part, divide the space into

TABLE 2. Typical values of parameters use in Back-Propagation algorithm.

Parameters	Symbol	Value
Neuron in the input layer	n	18
Neuron in the output layer	m	16
Neuron in the hidden layer	h	30
Coefficient of training	η	0.02

24 sectors and repeat every 15 degrees between 0° and 360° degrees inclusively. More exact space division sectors can be achieved by increasing the number of element arrays. A 24-bit binary code is used as the input vector for the neural network (one bit for each sector). A bin input of (+1) indicates a source in the sector that is exactly on (main lobe). Convergence could then be completed faster.

IV. RESULTS AND DISCUSSIONS
In this section, the simulation results of the optimized dual-band circular polarized BSPA antenna will be firstly presented, analyzed, and compared as the building block of the antenna array. Then, the UCA array simulation results will be offered to show their capabilities for steering the beam patterns in different directions.

A. ANTENNA DESIGN
The authors in this work present for the first time a design for the antenna called Bone-Shaped Patch Antenna (BSPA) that consists of several parts each one is considered for a specific function. The main objective is to resonate the antenna at 28 and 38 GHz simultaneously with an AR < 3 dB. Firstly, the shape of the sinusoidal bones has been studied as shown in Fig. 7a. It is found that changing the sinusoidal envelop shape effect directly on the antenna reflection coefficient and correspondingly on the antenna matching. Then the effect of the oval shape defected in the ground plane (DGS) is analyzed. The results revealed its effect on the antenna realized gain as presented in Fig. 7b, whereas, the larger DGS oval shape area leads to a higher realized gain value at the operating frequencies. Regarding the rhombus shape located in the middle of the antenna, it plays a major role in improving the antenna radiation efficiency as shown in Fig. 7c. Finally, the effect of radii bone ends has been studied as presented in Fig. 7d. Whereas, the circular polarity and the axial ratio of the antenna are greatly affected just by changing the direction of the bone shape in each group.

In order to generate a database for modeling the DNN, simulations of 150 BSPAs with various geometrical parameters are performed using CST-MWS [30]. The parameters of the simulated BSPAs are topologically illustrated in Fig. 8. The antenna parameters are considered in three ground plane slot dimensions $G_1 \times S_3$ groups of 10×3.6 mm^2, 9.3×3.5 mm^2, and 8.5×3 mm^2. Each group has 50 BSPAs that comprise a parameter combination of $G_1 \times S_3$. e.g. for the first group of 10×3.6 mm^2, there are 50 ESPAs including the parameter combination of (W$_{11}$: 3.5, 3.36, 3.22, 3.08, 2.94 mm) × (W$_{34}$: 3.5, 3.36, 3.22, 3.08, 2.94 mm) × (W$_{24}$: 3.5, 3 mm).
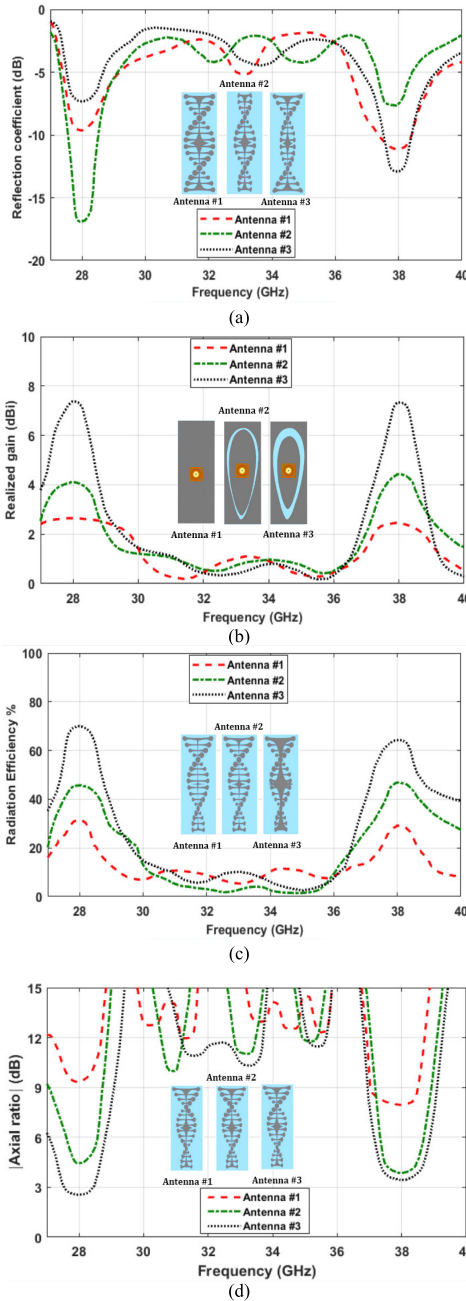
FIGURE 7. Test antennas radiation characteristics, (a) reflection coefficient, (b) realized gain, (c) radiation efficiency, and (d) axial ratio.

The simulated resonant frequency f_r of each BSPA with a particular antenna parameter is determined by CST.

Fig. 9 shows the simulated resonant frequency variation versus antenna number. Whereas the resonant frequencies decrease with the antenna ground plane slot dimensions, and hence there is a high nonlinearity between the antenna parameters and the resonant frequencies. Therefore, computing the resonant frequency of BSPA is a complex and high nonlinear problem. The simulations are performed between the frequency range of 28–38 GHz at 300 points.

According to the relationship between the input and the target, the DNN model with three layers was trained to produce
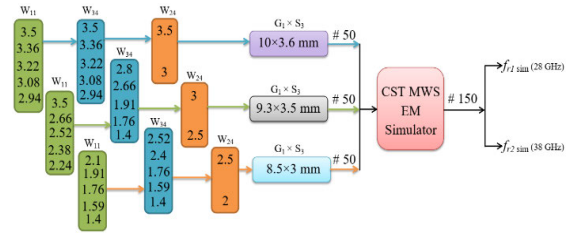

FIGURE 8. Topological illustration of the geometrical parameters of the simulated 150 BSPAs by CST 3D EM (dimension unit: mm).
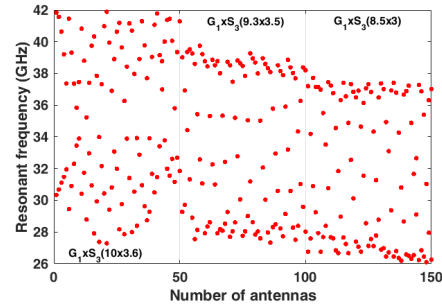

FIGURE 9. Simulated resonant frequency variation for each antenna group defined in Fig. 8.

the resonant frequency for each parameter set of the antenna. As many as 150 BSPAs were employed for training while 15 BSPAs were used for testing the DNN model. In order to visually recognize the relationships between the results, the scatter diagrams of simulated and computed resonant frequency results are shown in Fig. 10 for the training and testing datasets. The value of the average percentage errors (APE) for the resonant frequencies has been computed by the DNN model as depicted in Fig. 11 [37]. It is clear that, the APE value is affected by the assigned number of training points for any deep learning application. Whereas, the system accuracy improves by increasing the number of training points and vice versa. Based on Fig. 11, which illustrates the topology of calculating the APE for CST models, an appropriate APE of 0.236 % was obtained as for the 150 BSPAs' training data which increased to 1.587 by decreasing the training data to 72. It is clearly seen that the points will follow a linear pattern; means there is a high linear correlation between the results.

To further investigate the validity of the present approach, a BSPA operating at 28 and 38 GHz with the dimensions illustrated in Table 1 was designed via CST and then fabricated. These parameters not used in the training process, whereas, in the training data there is no antenna resonated simultaneously at 28 and 38 GHz as shown in the inset Fig. 10a. Fig. 12 shows a good agreement between the measured and simulated results. As shown in Fig. 12(a), the antenna can achieve good matching at both frequency bands to be −26.61 and −24.54 at 28 and 38 GHz, respectively, with realized gain of 8.97 and 8.65 dBi as depicted in Fig. 12b. Furthermore, the antenna had an axial ratio less than 3dB for $\theta = 90°$ and $\varphi = 0°$ at the resonance frequencies, in addition, as shown in Fig. 12c, the radiation efficiency is found to be 90.5 % and 87 % at 28 GHz and 38 GHz, respectively. Fig. 13 presents
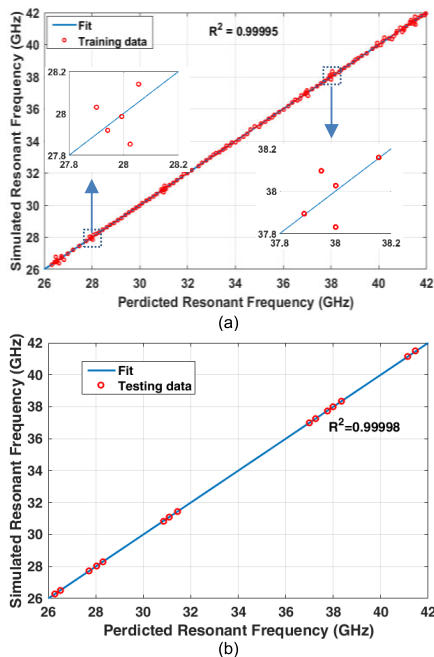
FIGURE 10. Scatter diagrams of the simulated and computed resonant frequency values by the DNN model for (a) Training data, (b) Test data.
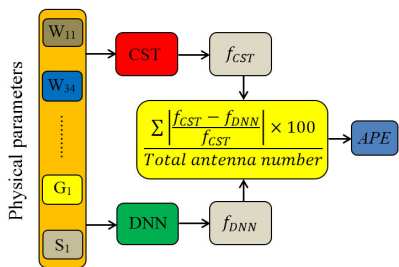

FIGURE 11. The topology of the calculating APE for CST models.

the simulated 3D radiation pattern of the optimized BSPA antenna at 28 and 38 GHz.

B. ANTENNA ARRAY

The proposed approach has been thoroughly tested as shown in Fig. 6, as seen by the examples below. For synthesizing the 16-element antenna array, the feeding voltages were set with constant amplitudes and variable phases [38], [39]. For the reference antenna, the predicted simulation results must demonstrate radiation patterns with low SLL (at −30 dB) and major lobes pointing in the direction of valuable signal. The desired radiation pattern is given from 0° to 360° in our application, and the database contains all the data (input/output) produced through simulation with the MGSA-PSO algorithm.

The proposed antenna array is analyzed using CST-MWS and linked with MGSA-PSO algorithm, MATLAB-coded, to optimize the antenna array phases. Accordingly, the following objective function is applied to achieve the goal. 24 desired directions of the UCA from 0° to 360° by step 15° were optimized by this objective function as a training data
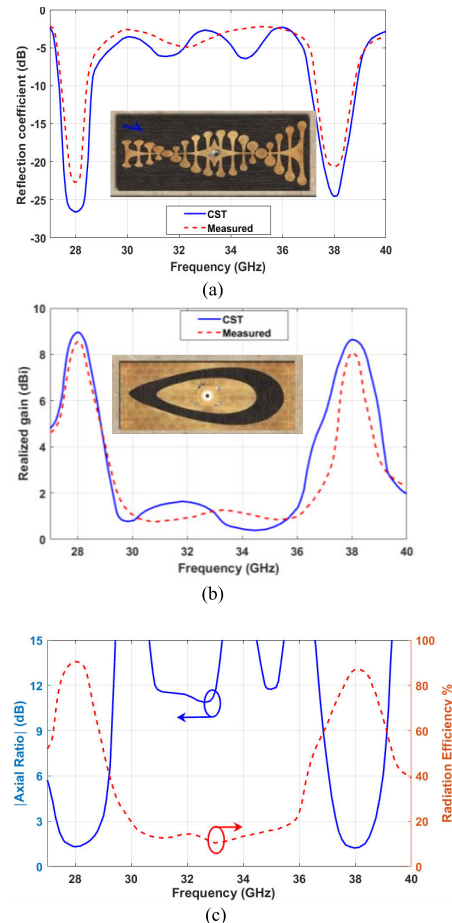

FIGURE 12. Antenna radiation characteristics, (a) reflection coefficient, (b) realized gain, (c) radiation efficiency and axial ratio. The inset figure illustrates the front and back view of fabricated antenna.
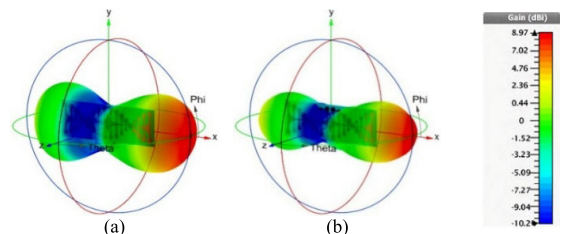

FIGURE 13. 3D far-field gain pattern at, (a) 28 GHz and (b) 38 GHz.

for DL mechanism.

$$Obj = \max |E_t (\theta_i, \varphi_i)| + \min(|SLL|_{dB} - 30) \quad (6)$$

The graphical output of the regression is shown in Fig. 14. The network outputs are placed against the targets as open circles. The best linear fit is indicated by a dotted line. The solid line indicates a perfect match (output equal to the targets). Because the fit is so superb in this case, it is difficult to tell the difference between the best linear fit line and the ideal fit line.

To demonstrate the effectiveness of the method identified in the previous section for steering single beams in the desired direction by controlling the phase excitation of each array element, 24 desired directions of the disc array with N = 16 elements were performed. In various settings, the numerical
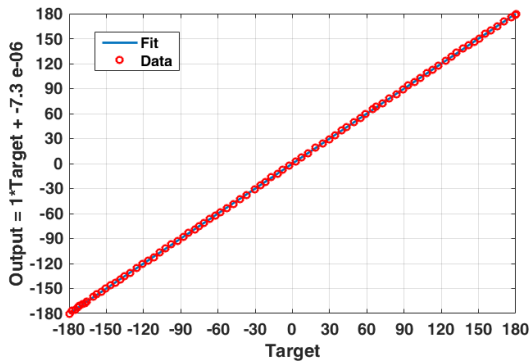
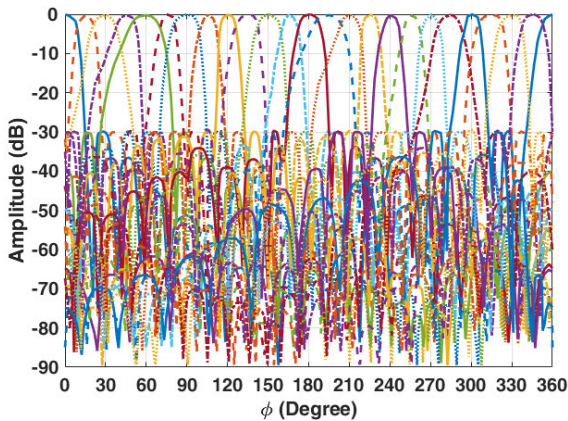**FIGURE 14.** Training state of the network created during training.

FIGURE 15. Radiation pattern of 16 elements λ =2 spaced array optimized using MGSA-PSO with respect to SLL (at −30 dB).

findings in Fig. 15 show that NNs with the MGSA-PSO algorithm have outstanding phase control capabilities for beam pattern synthesis. It is vital to test the neural network once it has completed the training phase on a different database than the one used for learning. This test allows you to evaluate the neural system's performance as well as identify the problematic data types. It will either update the network design or adjust the learning base if the performance is not adequate (each data class's distinguishing traits or representativeness).

Many examples of simulations are explored at $\varphi = 40°$, $142°$, $205°$, and $320°$, in order to test the proposed methodology for the synthesis of a circular disc array. It is evident that the side-lobe level requirement of $−30$ dB has been met. Fig. 16 shows the simulated results for 3D antenna radiation pattern synthesis using the DNN approach at 28 GHz for the built antenna array system with 16 elements. The results reveal that the desired and synthesized specifications are extremely closely aligned. This proves the recommended procedure's efficacy. This shows that the proposed procedures are effective. The DNN has superior learning, generalization, parallel processing, and error endurance properties, resulting in ideal solutions in applications where nonlinear mapping of complex data should be modelled. This method employs a DNN, which can be trained to handle any amount of elements, spacing, and excitation. The parameters with respect to the input can be found once the network has been trained.
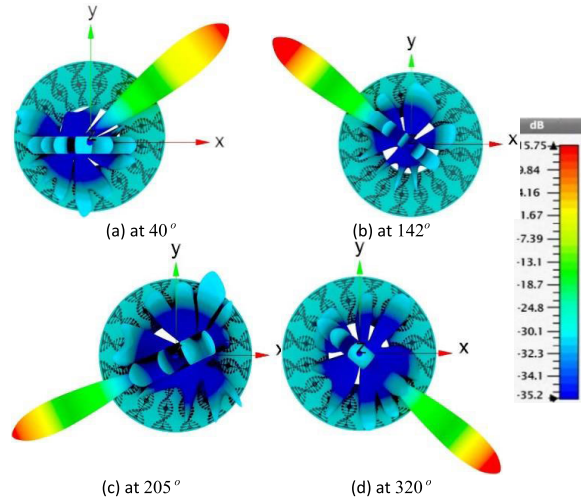

FIGURE 16. 3D Radiation pattern of several tested scenarios.

V. CONCLUSION

In this study, DNN is implemented to the computation of the resonant frequency of the BSPAs, and hence a DNN-based soft computing framework is modeled using a full-wave 3D EM analysis platform. The network is trained with a set of input-output data pairs based on MGSA-PSO algorithm. A database enclosing the resonant frequency of 150 BSPAs is defined by the simulations with different geometry and electrical parameters. For training and testing the model, the database is split into datasets #135 and #15, respectively. As a result, the proposed DNN model was used to estimate the resonant frequencies with the greatest precision, making it an efficient and potentially viable alternative to costly measurement and simulations. Then, the DNN model has applied to beam-steer the radiation pattern of the designed antenna array. Results show that there is an agreement between the desired specifications and the synthesized ones.

REFERENCES

[1] R. C. Hansen, *Phased Array Antennas*, vol. 213. Hoboken, NJ, USA: Wiley, 2009.

[2] I. Uchendu and J. R. Kelly, "Survey of beam steering techniques available for millimeter wave applications," *Prog. Electromagn. Res. B*, vol. 68, pp. 35–54, 2016.

[3] M. U. Afzal and K. P. Esselle, "Steering the beam of medium-to-high gain antennas using near-field phase transformation," *IEEE Trans. Antennas. Propag.*, vol. 65, no. 4, pp. 1680–1690, Apr. 2017.

[4] S. S. K. Puranam, A. Gopinath, and R. Sainati, "Amplitude based beam steering," in *Proc. IEEE Int. Symp. Phased Array Syst. Technol. (PAST)*, Oct. 2019, pp. 1–4.

[5] K. R. Mahmoud and A. M. Montaser, "Design of dual-band circularly polarised array antenna package for 5G mobile terminals with beam-steering capabilities," *IET Microw., Antennas Propag.*, vol. 12, no. 1, pp. 29–39, 2018.

[6] K. R. Mahmoud and A. M. Montaser, "Synthesis of multi-polarised upside conical frustum array antenna for 5G mm-wave base station at 28/38 GHz," *IET Microw., Antennas Propag.*, vol. 12, no. 9, pp. 1559–1569, Jul. 2018.

[7] K. R. Mahmoud and A. M. Montaser, "Performance of tri-band multi-polarized array antenna for 5G mobile base station adopting polarization and directivity control," *IEEE Access*, vol. 6, pp. 8682–8694, 2018.

[8] K. R. Mahmoud, A. Baz, W. Alhakami, H. Alhakami, and A. M. Montaser, "The performance of circularly polarized phased sub-array antennas for 5G laptop devices investigating the radiation effects," *Prog. Electromagn. Res. C*, vol. 110, pp. 267–283, 2021.

[9] K.-K. Yan and Y. Lu, "Sidelobe reduction in array-pattern synthesis using genetic algorithm," *IEEE Trans. Antennas Propag.*, vol. 45, no. 7, pp. 1117–1122, Jul. 1997.

[10] K. R. Mahmoud, M. I. Eladawy, R. Bansal, S. H. Zainud-Deen, and S. M. M. Ibrahem, "Analysis of uniform circular arrays for adaptive beamforming applications using particle swarm optimization algorithm," *Int. J. RF Microw. Comput.-Aided Eng.*, vol. 18, no. 1, pp. 42–52, Jan. 2008.

[11] E. Amed, K. R. Mahmoud, S. Hamad, and Z. T. Fayed, "Real time parallel PSO and CFO for adaptive beam-forming applications," in *Proc. PIERS*, Mar. 2013, pp. 25–28.

[12] K. R. Mahmoud and S. Hamad, "Parallel implementation of hybrid GSA-NM algorithm for adaptive beam-forming applications," *Prog. Electromagn. Res. B*, vol. 58, pp. 47–57, 2014.

[13] K. R. Mahmoud, "Synthesis of unequally-spaced linear array using modified central force optimisation algorithm," *IET Microw., Antennas Propag.*, vol. 10, no. 10, pp. 1011–1021, 2016.

[14] I. A. Basheer and M. Hajmeer, "Artificial neural networks: Fundamentals, computing, design, and application," *J. Microbiol. Methods*, vol. 43, no. 1, pp. 3–31, 2000.

[15] L. Alzubaidi, J. Zhang, A. J. Humaidi, A. Al-Dujaili, Y. Duan, O. Al-Shamma, J. Santamaría, M. A. Fadhel, M. Al-Amidie, and L. Farhan, "Review of deep learning: Concepts, CNN architectures, challenges, applications, future directions," *J. Big Data*, vol. 8, no. 1, pp. 1–74, Dec. 2021.

[16] A. B. Nassif, I. Shahin, I. Attili, M. Azzeh, and K. Shaalan, "Speech recognition using deep neural networks: A systematic review," *IEEE Access*, vol. 7, pp. 19143–19165, 2019.

[17] V. B. Semwal, K. Mondal, and G. C. Nandi, "Robust and accurate feature selection for humanoid push recovery and classification: Deep learning approach," *Neural Comput. Appl.*, vol. 28, no. 3, pp. 565–574, Mar. 2017.

[18] S. Ding, L. Guo, and Y. Hou, "Extreme learning machine with kernel model based on deep learning," *Neural Comput. Appl.*, vol. 28, no. 8, pp. 1975–1984, 2017.

[19] V. B. Semwal, K. Mondal, and G. C. Nandi, "Erratum to: Robust and accurate feature selection for humanoid push recovery and classification: Deep learning approach," *Neural Comput. Appl.*, vol. 28, no. 7, p. 1907, 2017.

[20] Y. Kim, "Application of machine learning to antenna design and radar signal processing: A review," in *Proc. Int. Symp. Antennas Propag. (ISAP)*, Oct. 2018, pp. 1–2.

[21] A. Massa, D. Marcantonio, X. Chen, M. Li, and M. Salucci, "DNNs as applied to electromagnetics, antennas, and propagation—A review," *IEEE Antennas Wireless Propag. Lett.*, vol. 18, no. 11, pp. 2225–2229, Nov. 2019.

[22] D. Erricolo, P.-Y. Chen, A. Rozhkova, E. Torabi, H. Bagci, A. Shamim, and X. Zhang, "Machine learning in electromagnetics: A review and some perspectives for future research," in *Proc. Int. Conf. Electromagn. Adv. Appl. (ICEAA)*, Sep. 2019, pp. 1377–1380.

[23] H. M. E. Misilmani, T. Naous, and S. K. A. Khatib, "A review on the design and optimization of antennas using machine learning algorithms and techniques," *Int. J. RF Microw. Comput.-Aided Eng.*, vol. 30, no. 10, pp. 1–28, Oct. 2020.

[24] L. Cui, Y. Zhang, R. Zhang, and Q. H. Liu, "A modified efficient KNN method for antenna optimization and design," *IEEE Trans. Antennas Propag.*, vol. 68, no. 10, pp. 6858–6866, Oct. 2020.

[25] M. Sarevska, "Signal detection for neural network-based antenna array," in *Proc. Conf. Circuits, Syst., Signals Marathon (NAUN)*, Attica, Greece, Jun. 2008, pp. 115–119.

[26] O. Barkat and A. Benghalia, "Optimization of superconducting antenna arrays using RBF neural network," *Int. J. Simul. Multidisciplinary Des. Optim.*, vol. 4, no. 1, pp. 7–10, Jan. 2010.

[27] A. Smida, R. Ghayoula, N. Nemri, H. Trabelsi, A. Gharsallah, and D. Grenier, "Phased arrays in communication system based on Taguchi-neural networks," *Int. J. Commun. Syst.*, vol. 27, no. 12, pp. 4449–4466, Dec. 2014.

[28] L. Merad, F. T. Bendimerad, S. M. Meriah, and S. A. Djennas, "Neural networks for synthesis and optimization of antenna arrays," *Radioengineering*, vol. 16, no. 1, pp. 23–30, Apr. 2007.

[29] J. H. Kim and S. W. Choi, "A deep learning-based approach for radiation pattern synthesis of an array antenna," *IEEE Access*, vol. 8, pp. 226059–226063, 2020.

[30] *Computer Simulation Technology Microwave Studio (CST MWS)*. Accessed: 2021. [Online]. Available: https://www.3ds.com/products-services/simulia/products/cst-studio-suite/

[31] I. Develi, "Application of multilayer perceptron networks to laser diode nonlinearity determination for radio-over-fibre mobile communications," *Microw. Opt. Technol. Lett.*, vol. 42, no. 5, pp. 425–427, 2004.

[32] S. Haykin, *Neural Networks: A Comprehensive Foundation*. New York, NY, USA: Macmillan, 1994.

[33] J.-S. R. JANG, "Self-learning fuzzy controllers based on temporal back propagation," *IEEE Trans. Neural Netw.*, vol. 3, no. 5, pp. 714–723, Sep. 1992.

[34] S. Kunis and D. Potts, "Time and memory requirements of the nonequispaced FFT," *Sampling Theory Signal Image Process.*, vol. 7, no. 1, pp. 77–100, Jan. 2008.

[35] G. Castaldi, V. Galdi, and G. Gerini, "Evaluation of a neural-network-based adaptive beamforming scheme with magnitude-only constraints," *Prog. Electromagn. Res. B*, vol. 11, pp. 1–14, 2009.

[36] K. A. Gotsis, K. Siakavara, and J. N. Sahalos, "On the direction of arrival (DoA) estimation for a switched-beam antenna system using neural networks," *IEEE Trans. Antennas Propag.*, vol. 57, no. 5, pp. 1399–1411, May 2009.

[37] A. Akdagli, A. Toktas, A. Kayabasi, and I. Develi, "An application of artificial neural network to compute the resonant frequency of E-shaped compact microstrip antennas," *J. Electr. Eng.*, vol. 64, no. 5, pp. 317–322, Sep. 2013.

[38] D. Vakula and N. V. S. N. Sarma, "Using neural networks for fault detection in planar antenna arrays," *Prog. Electromagn. Res. Lett.*, vol. 14, pp. 21–30, 2010.

[39] S. Reza and C. G. Christodoulou, "Beam shaping with antenna arrays using neural networks," in *Proc. IEEE South East Conf.*, Orlando, FL, USA, Apr. 1998, pp. 220–223.

AHMED M. MONTASER received the B.S. and M.S. degrees in communications and electronics engineering from South Valley University, Aswan, Egypt, in 2003 and 2009, respectively, and the Ph.D. degree from Mansoura University, Egypt, in 2013. He is currently an Associate Professor with the Department of Communication and Electronics, Faculty of Technology and Education, Sohag University, Sohag, Egypt. He authored more than 30 papers on microwave based smart antenna, conformal array devices, and mmWave antennas. His current research interests include the areas of microwave applications in biomedical, especially in breast and brain cancer, hyperthermia, and using millimeter wave for cancer detection. He has served as an Editor/Reviewer of many international journals.

KORANY R. MAHMOUD (Senior Member, IEEE) received the B.S. and M.S. degrees in communications and electronics engineering from Helwan University, in 1998 and 2003, respectively, and the Ph.D. degree from Helwan University in collaboration with the University of Connecticut, USA, in 2008. He is currently a Professor with the Department of Communications and Electronics Engineering, Helwan University. He is also the Vice Dean of Community Service and Environmental Development. Since 2012, he has been worked as the Research and Development Director of the National Telecommunications Regulatory Authority (NTRA), Egypt. He has published over 80 refereed journal and conference papers in addition to one book on reconfigurable microwave filter. His current research interests include the areas of 5G mm-wave and optical nano-antennas design for modern wireless applications using meta-heuristic optimization techniques, and microwave hyperthermia, microwave filters design, and radar cross section reduction techniques.

● ● ●